Agricultural and Forest Meteorology 308–309 (2021) 108609

Contents lists available at ScienceDirect

Agricultural and Forest Meteorology

journal homepage: www.elsevier.com/locate/agrformet

Land cover change-induced decline in terrestrial gross primary production over the conterminous United States from 2001 to 2016

Yulong Zhang[a,b,*], Conghe Song[a,*], Taehee Hwang[c], Kimberly Novick[d], John W. Coulston[e], James Vose[e], Matthew P. Dannenberg[f], Christopher R. Hakkenberg[g], Jiafu Mao[h], Curtis E. Woodcock[i]

[a] Department of Geography, University of North Carolina at Chapel Hill, Chapel Hill, NC, United States
[b] Institute for a Secure and Sustainable Environment (ISSE), University of Tennessee, Knoxville, TN, United States
[c] Department of Geography, Indiana University, Bloomington, IN, United States
[d] O'Neill School of Public and Environmental Affairs (SPEA), Indiana University, Bloomington, IN, United States
[e] Eastern Forest Environmental Threat Assessment Center, USDA Forest Service, Raleigh, NC, United States
[f] Department of Geographical and Sustainability Sciences, University of Iowa, Iowa City, IA, United States
[g] School of Informatics, Computing, and Cyber Systems, Northern Arizona University, Flagstaff, AZ, United States
[h] Environmental Sciences Division and Climate Change Science Institute, Oak Ridge National Laboratory, Oak Ridge, TN, United States
[i] Department of Earth and Environment, Boston University, Boston, MA 02215, United States

A R T I C L E I N F O

Keyword:
Land cover change (LCC)
Gross primary production (GPP)
National land cover database (NLCD)
Google earth engine (GEE)
TRENDY
CONUS

A B S T R A C T

As one of the most dynamic aspects of global environmental change, land cover change (LCC) has a profound impact on terrestrial carbon sequestration. However, LCC-induced carbon fluxes are still the most uncertain terms in global and regional carbon budgets. Ecosystem gross primary production (GPP) is the total carbon uptake by vegetation through photosynthesis, serving as a major control on ecosystem function and land carbon balance during and after the modification of the land surface. However, accurately capturing LCC-induced GPP changes requires both high-quality land cover data and controlling for variation driven by other environmental factors such as climate. In this study, we comprehensively examined the effects of LCC on annual GPP trends over the conterminous United States (CONUS) from 2001 to 2016 using the USGS National Land Cover Database, a remote sensing-driven ecosystem model, and the Google Earth Engine cloud computing platform. We designed a series of model experiments to identify LCC effects on GPP by controlling climate effects. During the study period, LCC exerted a strong negative effect on total GPP across the CONUS ([-2.2, -1.8] Tg C yr^{-2}), while climate had smaller positive effects ([0.17, 0. 92] Tg C yr^{-2}). The LCC-induced reduction of GPP was mainly caused by net forest loss ([-1.98, -1.39] Tg C yr^{-2}) and urban expansion ([-2.03, -1.92] Tg C yr^{-2}), but was partially offset by increases in crop area ([+0.66, +0.79] Tg C yr^{-2}). Ensemble simulations from TRENDY did not capture the strong negative LCC influences on GPP, likely due to limitations of the adopted land use/cover data. Our study provides a novel perspective on LCC-induced GPP changes, which could help to improve our understanding of ecosystem function changes and constrain the estimation of land carbon balance in the context of anthropogenic activity and climate change.

1. Introduction

Land cover change (LCC) caused by anthropogenic activity through land use change and natural disturbances represents one of the most dynamic aspects of global environmental change, which has profound impacts on land carbon sequestration in the context of climate change (Foley, 2005; Pielke, 2005; Zhang et al., 2019; Piao et al., 2020). The terrestrial biosphere acts as a major carbon sink in the global carbon cycle (Falkowski et al., 2000), potentially offsetting one third of fossil fuel emissions (Le Quéré et al., 2018; Friedlingstein et al., 2019). However, an equivalent of about half of the total land carbon sink is reemitted back into the atmosphere through LCC primarily related to deforestation (Friedlingstein et al., 2019). After fossil fuel emissions, LCC is the second largest contributor of anthropogenic emissions to the

* Corresponding authors.
E-mail addresses: ylzhang@utk.edu (Y. Zhang), csong@email.unc.edu (C. Song).

https://doi.org/10.1016/j.agrformet.2021.108609
Received 3 December 2020; Received in revised form 24 July 2021; Accepted 8 August 2021
Available online 18 August 2021

atmosphere. Nevertheless, compared to fossil fuel emissions and other components of the global carbon budget, LCC-induced carbon emissions are associated with the highest uncertainty (Houghton et al., 2012; Sitch et al., 2015; Arneth et al., 2017; Friedlingstein et al., 2019).

Ecosystem gross primary production (GPP) is the total carbon uptake by vegetation through photosynthesis (Beer et al., 2010), serving as a primary regulator of the land carbon balance by offsetting potential carbon releases during and after LCC (Hansis et al., 2015). Therefore, constraining LCC-induced GPP change could provide a better understanding of ecosystem function (Anav et al., 2015; Zhang et al., 2014, 2019) and further reduce uncertainties in global and regional carbon balances (Erb et al., 2013; Arneth et al., 2017). This goal is also aligned with recently renewed efforts to understand the role of LCC in implementing "natural climate solutions" (Griscom et al., 2017; Fargione et al., 2018).

While globally important, LCC typically occurs locally and across various vegetation types and climate zones (Sleeter et al., 2013). Precisely quantifying the influence of LCC on GPP relies on robust ecosystem models with spatially explicit land cover data that can characterize the type, location, extent, and frequency of LCC at fine spatial scales. Global or national-scale LCC-induced carbon fluxes are usually estimated in a simplified manner through bookkeeping models (Coulston et al., 2015; Friedlingstein et al., 2019), which incorporate straightforward carbon accounting methods based on forest inventory, agricultural statistical and/or social census data (e.g., FAOSTAT; http://www.fao.org/faostat). Consequently, they do not include transient responses of ecosystems to environmental changes and most of them lack spatial details of land use/cover change influences (Houghton et al., 2012; Pongratz et al., 2014; Obermeier et al., 2021). Meanwhile, process-based dynamic global vegetation models (DGVMs) have been used to quantify LCC effects on GPP, for example, based on century-long harmonized land use data (e.g., HYDE, LUH2, Anav et al., 2015; Arneth et al., 2017). Although DGVMs can simulate carbon dynamics with detailed biogeochemical processes, the demand for sophisticated high-quality model inputs is usually hard to satisfy and their operational spatial resolutions (0.25° - 1°) are usually too coarse to evaluate the effects of fine-scale LCC (Anav et al., 2015; Bastos et al., 2020). Consequently, comparisons of simple bookkeeping models against process-based models (e.g., TRENDY; Sitch et al., 2015) still reveal large discrepancies in the estimation of LCC-induced carbon fluxes (Friedlingstein et al., 2019; Bastos et al., 2020; Harris et al., 2021).

Satellite observations allow near real-time, large-scale monitoring of land surface conditions (Song et al., 2015), facilitating not only the derivation of high frequency land cover information (ESA, 2017; Dannenberg et al., 2018; Sulla-Menashe et al., 2019) but also vegetation status during or after disturbances (Frolking et al., 2009; Didan et al., 2015). Remote sensing driven ecosystem models, such as those derived from light-use efficiency theory, provide an alternative approach for quantifying fine-scale LCC-induced GPP change (Zhang et al., 2014). Combined with fine-resolution land cover datasets, such as those provided by the USGS National Land Cover Database (NLCD) (Homer et al., 2020), these models have the potential to better constrain LCC-induced changes in GPP at the scale at which LCC occurs (i.e., local to regional scales).

The conterminous United States (CONUS) possesses diverse ecosystems and heterogenous landscapes but has experienced intensive LCC related to anthropogenic and natural disturbance over the past two decades (Dannenberg et al., 2018; Homer et al., 2020). However, the patterns, magnitudes, and rates of LCCs and their corresponding influences on carbon fluxes remain debatable (Arneth et al., 2017; Yu et al., 2019; Liu et al., 2020). For example, the national inventory data of FAOSTAT and global harmonized land cover data (Hurtt et al., 2017) showed an increase of total forest area but a decrease of cropland area over the CONUS since 2001, which contradict remote sensing-based observations (Hansen et al., 2013; ESA, 2017; Li et al., 2018). Accordingly, the land carbon sink over the CONUS may be largely overestimated without critical fine-scale LCC information (Liu et al., 2020) or even turned to carbon source after accounting for more accurate LCC information (Yu et al., 2019).

The NLCD provides more than two decades of comprehensive land cover information at a 30-m spatial resolution over the CONUS (Fry et al., 2008; Yang et al., 2018). However, early versions of the NLCD are not quite suitable for LCC analysis due to data inconsistency (i.e., before and after 2000), relative low cyclical updates, and a short accumulation period (e.g., only a decade for NLCD 2011 with a five-year interval) (Fry et al., 2008; Homer et al., 2015). The recent release of NLCD (2016) represents a next generation NLCD product with a consistent multi-temporal land cover database at 2-3-year intervals since 2001 (Yang et al., 2018). Thus, the newly updated NLCD provides a chance to re-evaluate the status of LCC over the CONUS and its contributions to changes in land carbon fluxes.

Here, we assimilated the newly released NLCD into a remote sensing-driven ecosystem model in Google Earth Engine (GEE) to examine the spatiotemporal patterns of LCC over the CONUS and further isolate the effects of LCC on annual GPP trends from climate change and variability using factorial model simulations. Specifically, we addressed four scientific questions: (1) What were the spatial/temporal patterns of LCC over the CONUS from 2001 to 2016? (2) How did LCC affect terrestrial GPP at national/regional scales and by LCC type? (3) How different were the influences of LCC compared to those from climate variability and change? (4) To what extent did ensemble model simulations from TRENDY capture LCC-induced GPP changes identified in the analysis of the NLCD database? By answering these questions, our study would offer a novel perspective on the dominant modes of LCC-driven GPP change across the CONUS, beyond which informing model predictions is also highly relevant for ongoing efforts to sustain the US terrestrial carbon sink.

2. Materials and Methods

2.1. CCW model

We used the Coupled Carbon and Water (CCW) model to estimate the respective effects of LCC and climate change on GPP. The CCW is a recently developed diagnostic ecosystem model based on global eddy flux tower and remote sensing data (Zhang et al., 2016, 2019). In CCW, GPP is estimated as the product of absorbed photosynthetically active radiation (APAR) and realized LUE ($\mathscr{E}$) that varies with vegetation type and climate based on light-use efficiency (LUE) theory:

$$GPP = APAR \times \mathscr{E} = (PAR \times FPAR) \times \varepsilon_{pot} \times f(E) \tag{1}$$

where PAR is the incident photosynthetically active radiation (MJ m^{-2}), which is assumed to be 45% of the total short-wave radiation; FPAR is the fraction of PAR absorbed by plants, which is linearly related to remote sensing-based normalized difference vegetation index (NDVI) (Sims et al., 2005); $\varepsilon_{\mathrm{pot}}$ (g C MJ^{-1}) is the potential LUE without environmental stresses; and $f(E)$ represents scalar functions that reduce LUE in responses to environmental stress. CCW accounts for environmental stress effects from diffuse radiation (R_s), temperature (T_s) and water stresses (W_s):

$$f(E) = R_s \times T_s \times W_s \tag{2}$$

$$R_s = 1 - K_1 \times CI \tag{3}$$

$$T_s = \frac{(T - T_{min}) \times (T - T_{max})}{(T - T_{min}) \times (T - T_{max}) - \left(T - T_{opt}\right)^2} \tag{4}$$

$$W_s = e^{-K_2 \times (VPD - VPD_{min})} \tag{5}$$

where CI is a clear-sky index (defined as the ratio of actual radiation to clear-sky radiation); K_1 is a diffuse light response parameter in which a smaller K_1 indicates a stronger influence of diffuse radiation on LUE; T is the monthly mean air temperature; T_{min}, T_{max} and T_{opt} are the minimum, maximum and optimal air temperatures for photosynthetic activity, respectively; VPD is the monthly vapor pressure deficit (hPa); K_2 is a moisture sensitivity parameter, whereby a higher K_2 indicates a larger reduction of LUE in response to VPD; and VPD_{min} is the minimum VPD above which moisture stress starts to take effect. W_s is set to 1.0 when the VPD is lower than VPD_{min}.

The parameters ε_{pot}, T_{min}, T_{max}, T_{opt}, K_1, and K_2 are biome-specific (Table S1) and have been calibrated based on global flux tower data from FLUXNET2015 and remote-sensing based NDVI from MODIS-C6 (Zhang et al., 2019). Additional details about the theoretical framework and model validation at multiple levels (i.e., site-, biome- and spatial-levels) can be found in previous studies (Zhang et al., 2016, 2019). Overall, CCW explained 71% of the variation in tower-based GPP with a root-mean-square error of 2.0 g C m^{-2} day^{-1}, which is comparable to most existing remote sensing-based models of GPP (Zhang et al., 2019). In addition, the biome-specific parameters, simplified yet robust model structure, and consideration of key environmental constraints from temperature, water stress and light saturation all make CCW particularly useful for examining the LCC effects on GPP separately from climate change effects at broad scales (Zhang et al., 2019).

2.2. Driver datasets for CCW

To drive CCW, we used all epochs of 30-m land cover data from NLCD 2016, 16-day 250-m NDVI from MODIS (i.e., MOD12Q1 C6) (Didan et al., 2015), and monthly 1 km climate data from Daymet3 (Thornton et al., 2017) from 2001 to 2016.

2.2.1. Land cover data

Based on the Landsat images and a series of ancillary land products, the United States Geological Survey recently updated the 30-m NLCD to a newer version (i.e., NLCD 2016) with innovative, consistent and robust methodologies (Jin et al., 2019). Different from previous versions of the NLCD at 5-10 year intervals, NLCD 2016 offers multi-temporal land cover data at 2-3 year intervals between 2001 and 2016 (Yang et al., 2018). The overall accuracy of 82% - 86% for the NLCD 2016 (Yang et al., 2018; Jin et al., 2019) outperforms existing global land cover products: e.g., 73.6% for MCD12Q1 (Sulla-Menashe et al., 2019), 72-75% for ESA-CCI (ESA, 2017), and 80% for GLOBELAND30 (Chen et al., 2015).

All seven epochs of land cover data from NLCD 2016 (i.e., 2001, 2004, 2006, 2008, 2011, 2013 and 2016) were utilized in this study. For those missing years, the closest land cover data were used for gap-filling. The original NLCD land types were regrouped into 9 classes, including evergreen forest, deciduous forest, mixed forest, shrub, grass (grassland/herbaceous and pasture/hay), crop, urban, barren, and water/wetland. In this study, since we mainly focused on the GPP dynamics over terrestrial ecosystems, aquatic or semi-aquatic ecosystems related to water/wetlands were masked out. The remaining non-vegetated types (i.e., urban & barren) were incorporated for LCC analysis, but their GPP values were set to zero in the CCW.

For comparison to our NLCD 2016 analysis, we further collected annual 500-m MODIS Land Cover Product (Collection 6 MCD12Q1) and annual 300-m ESA-CCI Land Cover Data for the period from 2001 to 2016. We selected the classification scheme of International Geosphere-Biosphere Programme (IGBP) in MCD12Q1 to compare with the NLCD 2016. The ESA-CCI land cover data, which adopts a classification from the United Nations-Land Cover Classification System, was converted to the IGBP in this study (Zhang et al., 2019). In addition, annual national inventory data from FAOSTAT (http://www.fao.org/faostat/en) and 0.25° Land Use Harmonization data (LUH2v2.1h) (Hurtt et al., 2017) for years corresponding to the study period were included for comparison to our NLCD 2016 analysis.

2.2.2. Vegetation index data

The 16-day 250-m MODIS NDVI product (i.e., MOD12Q1 C6) over the CONUS was used to drive the CCW over the study period (2001-2016). The collection 6 MODIS NDVI was retrieved from daily, atmosphere-corrected, bidirectional surface reflectance (Didan et al., 2015), and issues of sensor degradation in the prior collection 5 were largely resolved (Zhang et al., 2017). Based on the detailed quality control flag, poor-quality NDVI values (mostly related to clouds, aerosols, snow/ice and bad geometry etc.) were linearly interpolated based on the closest good-quality data within a window of 64 days. If no good quality NDVI values were found within this window, the multiple-year average of high-quality 16-day values was used. Where the 16-day averaged data was still unavailable, monthly averaged high-quality data were used. After the 16-day smoothed series was constructed, the monthly average of NDVI was then calculated as the input to the CCW. Note that, to better serve our purpose of separating LCC effects from climate change, we chose the NDVI-based FPAR model (Sims et al., 2005) rather than MODIS-C6 FPAR product (https://lpdaac.usgs.gov/products/mcd15a2hv006/), largely because current MODIS-C6 FPAR product is modelled based on a static multi-year land cover product from MOD12Q1. Therefore, land cover change information over shorter (annual) timescale may not be captured by the MODIS FPAR product. In addition, the inextricable coupling of the MODIS FPAR with the MODIS land cover product may preclude the use of other higher-quality land cover products (such as NLCD) in simulating LCC influences.

2.2.3. Climate data

We obtained daily shortwave solar radiation, air temperature, and VPD from 1-km Daymet V3, which was derived from in-situ meteorological observations and various supporting datasets over North America (Thornton et al., 2017). We calculated VPD from daily minimum/maximum air temperature and actual water vapor pressure (Allen et al., 1998). All daily variables were aggregated to monthly values for model simulation. To calculate clear-sky solar radiation, we adopted a 30-m DEM from GMTED2010 (Danielson & Gesch, 2011).

2.2.4. Model implementation in Google Earth Engine

We implemented the CCW model in Google Earth Engine (GEE), a cloud-based geospatial processing platform, which has been widely used for large-scale environmental monitoring and modeling (Gorelick et al., 2017; Tamiminia et al., 2020). To balance computing efficiency, output storage, and input data quality, all the input data were resampled to a spatial resolution of 300 m. Among them, NLCD was upscaled based on the majority rule, while other data were interpolated based on the nearest neighbor method.

2.3. Modeling design

To disentangle the effects of LCC and climate change on GPP, we designed three groups of simulation scenarios based on different combinations of model inputs (Table 1). The first group ("All") was assembled to produce the actual ensemble GPP dynamics by allowing all model inputs to change with time. The second group simulated LCC effects on GPP, including two simulations, S1 and S2. S1 held land cover at the initial 2001 level, but allowed all other variables to change, while S2 further held FPAR at the 2001 level. We used the simulation difference between All and S1 ("LCC1") to represent the direct effect of LCC on GPP independent of climate change effects. In CCW, land cover type determines the biome-specific potential LUE and other sensitivity parameters to climate variables. However, LCC1 did not account for the potential effect of FPAR change caused by LCC. Therefore, we further considered this effect using the simulation difference between All and S2 ("LCC2"), which represents the integrated effect of LCC. The realistic LCC effect on GPP can be constrained by LCC1 and LCC2. To quantify climate effects, two additional simulations (S3 and S4) were conducted. S3 allowed land cover and FPAR to change but held all three climate

Table 1
Scenario designs to disaggregate land cover change (LCC) and climate change effects on GPP based on CCW. The symbol '△' indicates that the input variable changes along time, while the symbol '▲' indicates that the input variable is fixed as the level in the initial year. The LCC effect is constrained by the direct LCC effect from LCC1 (i.e., All – S1) and indirect LCC effect from LCC2 (i.e., All – S2), while climate change effect is constrained by the direct effect from CLM1 (i.e., All – S3) and indirect effect from CLM2 (i.e., All – S4).

Group	All	Land Cover Change (LCC)		Climate Change	
	-	LCC1	LCC2	CLM1	CLM2
	-	All – S1	All - S2	All – S3	All – S4
Simulation	All	S1	S2	S3	S4
Land Cover	△	▲	▲	△	△
FPAR	△	△	▲	△	▲
Radiation	△	△	△	▲	▲
Temperature	△	△	△	▲	▲
VPD	△	△	△	▲	▲

factors (solar radiation, air temperature and VPD) at the initial 2001 level, while S4 only allowed land cover to change with time but held all the other factors constant. The simulation difference of All – S3 ("CLM1") reflects the direct effect of climate change on GPP, while All – S4 ("CLM2") further includes the partial effect of climate change on FPAR change, and thus GPP change (Table 1). Therefore, the realistic climate effect on GPP can be constrained by CLM1 and CLM2.

2.4. Analysis methods

To conduct LCC-related analyses, we first identified stable and change areas in land cover by stacking all NLCD data together. Pixels were labeled as stable areas if they did not experience change across NLCD dates. Otherwise, pixels were labeled as change areas. Any pixels classified as water or wetlands during the study period (accounting for 8% of total CONUS area) were excluded from further analysis. By comparing the initial NLCD in 2001 and the ending NLCD in 2016, a land cover transition matrix over the CONUS was calculated, and major LCC types (including deforestation, reforestation, crop expansion, crop shrinkage, and urbanization) were identified over five sub-regions (i.e., Northwest, Midwest, Northeast, Southwest and Southeast). After that, annual GPP trends from different model simulations were analyzed and subsequent LCC and climate change effects on GPP were assessed. It is worth noting that our NLCD-based study is only focused on the land cover change areas related either to natural disturbances or anthropogenic activities. Those stable land-cover areas with land-use and management changes (e.g., change of crop types), but not captured by NLCD, were excluded in our study.

Given the incomplete series of NLCD data with 2- or 3-years interval, we conducted two more scenario simulations (i.e., "early" LCC and "late" LCC) to evaluate the uncertainty of the group simulation based on the nearest neighbor gap-filling method (seen in Section 2.2.1). In the extra simulations of "early" and "late" LCC, the potential conversion years are fixed as the first year and last year in the intertwining years, respectively. For example, assuming a pixel changed from forest in 2001 to grass in 2004 in the NLCD data, the conversion year for the "early" LCC is assigned as the first year (i.e., 2002), while the "late" LCC is realized in the last year (i.e., 2004). Therefore, the range of GPP affected by conversion years could be constrained by these two extreme group scenarios. All other LCC patterns should fall between these two extreme cases, which provide the range of uncertainty caused by the timing of LCC on GPP.

2.5. TRENDY data

To examine if land surface models capture the fine-scale LCC-induced GPP changes identified in this study, we further examined GPP simulations from TRENDY (Version 7) during the study period. TRENDY contains ensemble results from multiple DGVMs and have been used to quantify the effects of common historical forcing on global ecosystem dynamics (Sitch et al., 2015; Quéré et al., 2018). Based on TRENDY factorial simulations, we calculated LCC-induced GPP changes based on differences between S3 (i.e., CO_2, climate, and land use change along time) and S2 (i.e., only CO_2 and climate change). Here we included 6 of 16 models from TRENDY V7 in our analysis (Table S2) because the remaining models are not comparable with the simulations in this study due to the additional modeling of nitrogen effect in S3. The spatial resolutions of model outputs from TRENDY vary from $0.5 \times 0.5\,^{\circ}$ to $2 \times 2\,^{\circ}$ (Table S2). To be consistent in the analysis, all TRENDY outputs were resampled to $1 \times 1\,^{\circ}$.

The land cover data used in TRENDY V7 was adopted from the yearly Land Use Harmonization data (LUH2; version 2.1h) at a spatial resolution of $0.25 \times 0.25\,^{\circ}$ (Quéré et al., 2018). To further evaluate the potential difference between TRENDY and NLCD-based simulations, we conducted simulations of LCC-induced GPP dynamics based on the fractional land use/cover state from LUH2 and the CCW model following the scenarios in Table 1. Given TRENDY accounts for land-use change and management practices over the stable land-cover areas (e.g., cropland), which are not explicitly considered in our analysis described here, we only focused on the evaluation of TRENDY and LUH2 simulations over the land-cover change area identified by NLCD. Due to the spatial resolution difference (0.25-degree vs 300-m), we generated statistics in two ways: 1) aggregating the fine-scale 300-m NLCD change area mask to match the original resolution of LUH2 (0.25-degree); 2) interpolating the coarse $0.25 \times 0.25\,^{\circ}$ LUH2 simulations to 300×300 m to match the resolution of the fine-scale NLCD change area mask.

Given LUH2 mainly represents anthropogenic land use change rather than natural disturbances (such as wildfire), we further evaluated the potential discrepancy of LCC effects on GPP between NLCD and LUH2 simulations over fire and non-fire regions. The spatial distribution of all wildfires during 2001 to 2016 over CONUS were derived from the national 30-m Monitoring Trends in Burn Severity (MTBS; https://www.mtbs.gov/project-overview). Overall, 20.4% of land change area identified by NLCD is related to fire disturbance (Fig. S1), which has been included in our analysis.

3. Results

3.1. Spatial & temporal patterns of land cover change over the CONUS

Based on all seven epochs of NLCD data, 7.9% of the total area of the CONUS (excluding water/wetlands; same hereafter) experienced land cover changes at least once during the study period (Fig. 1), corresponding to 567,950 km^2, or an area larger than California. Those changes primarily occurred in areas that were classified as forest (41% of total change area), grass (31% of total change area) and shrubland (24% of total change area) in 2001 (Fig. 1c). From 2001 to 2016, forests showed the largest decrease in area (equivalent to 0.86% of the total area or 10.8% of total change area), followed by grassland (4.3% of total change area) (Fig. 1d). In contrast, cropland showed the largest increase in area (9.7% of total change area), followed by urban (4.7% of total change area) (Fig. 1d). Shrub and barren/ice areas showed relatively small changes. Note that different land cover types showed different inter-annual variabilities (Fig. 1d). Overall, the changing rates of forest and urban areas tended to level off over time, while cropland showed an accelerated increase.

From 2001 to 2016, forest losses occurred in 27.2% of the total change area, mainly due to transitioning to grass (12.8%) and shrub (12.2%) (Fig. 2a). Concurrently, forest gains were observed in 16.4% of the change area, largely due to conversions from grass (8.4%) and shrub (7.3%). Although net shrubland change was small (0.7%), it had large gross gains (19.7%) and losses (19.0%), mostly related to grass and forest conversions (Fig. 2a). During this period, only 3.2% of the total change area showed crop losses, but 12.9% of the total change area

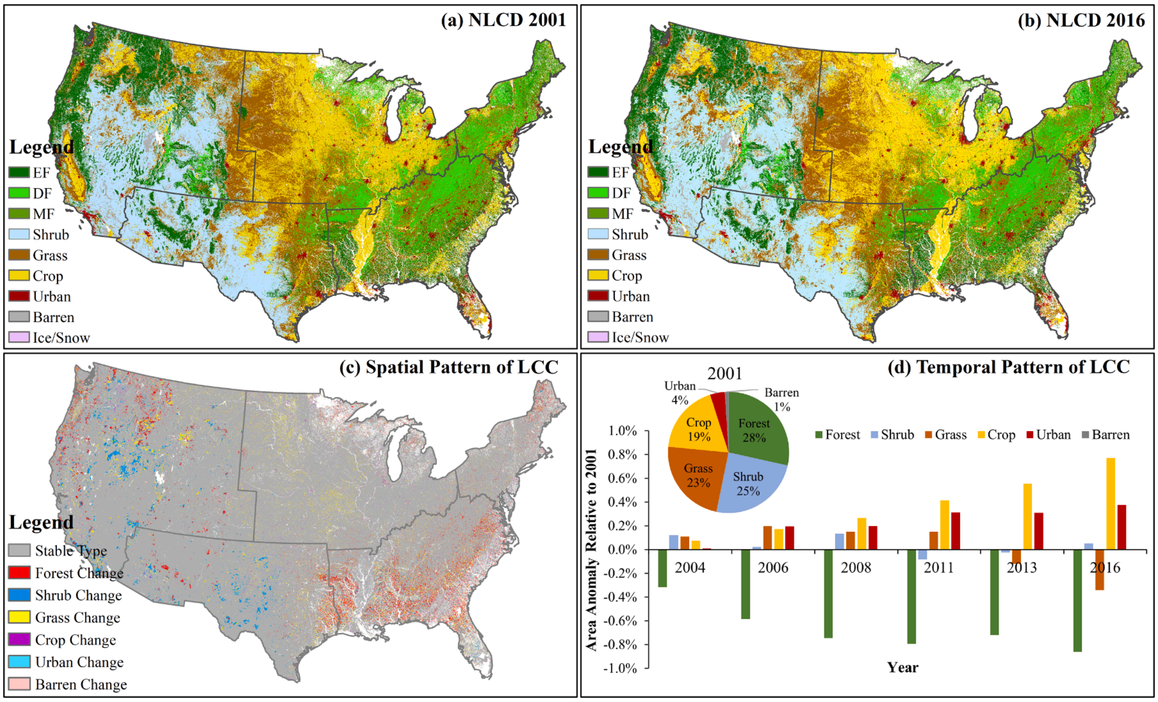

Fig. 1. Spatial and temporal patterns of land cover change (LCC) over the CONUS from 2001 to 2016. (a) ~ (c) show spatial patterns of land cover from NLCD 2001, NLCD 2016 and LCC between them (i.e., base year: 2001; ending year: 2016), respectively; (d) shows temporal pattern of LCC relative to the year of 2001. All water and wetlands are masked out in (a) ~ (d). Abbreviations in (a) & (b): EF (evergreen forest), DF (deciduous forest) and MF (mixed forest); The proportion in pie chart in (d) is relative to the total area of CONUS.

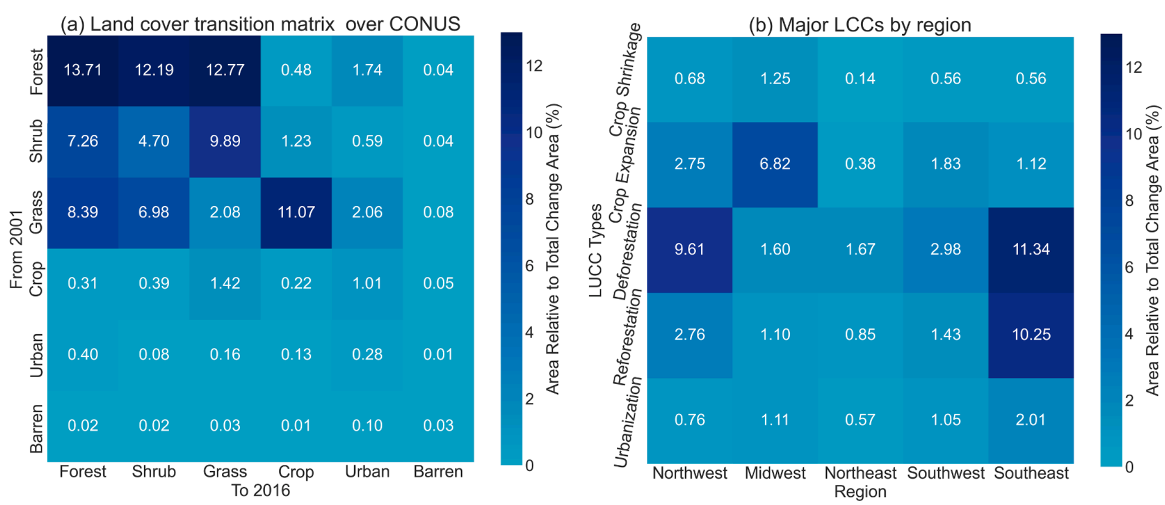

Fig. 2. Land cover transition matrix over the CONUS (a) and major land cover changes (LCCs) by regions (b) from 2001 to 2016. Numbers in (a) and (b) represent proportions of total change area.

exhibited crop gains, mainly at the expense of grass (Fig. 2a). Similarly, urban losses represented a very small fraction (0.8%) of the total change area, but urban gains from forest and grass were relatively large (4.7%). Interestingly, all land cover types showed a certain portion in the disturbed area (0.03% ~ 13.7% of the total change area), which indicate each land-use/land-cover class had at least one disturbance event within the study period. At the regional scale, both forest losses and forest gains were mainly located in the Southeast and Northwest (Fig. 2b). Crop expansion and urbanization was mainly found in the Midwest and Southeast, respectively (Fig. 2b).

3.2. *Effects of land cover change on GPP across cover change types*

We evaluated the effects of LCC, independent of climate effects, on annual GPP trends using the LCC1 (accounting for direct land cover change) and LCC2 (further accounting for LCC-induced canopy function change) model simulations (Table 1; Fig. 3). Over the CONUS, forest losses exerted a strong negative effect on GPP (i.e., [-4.69, -2.90] Tg C yr^{-2}; range given by LCC1 and LCC2, same hereafter), primarily due to the conversions to shrub ([-2.50, -1.96] Tg C yr^{-2}), grass ([-1.20, -0.07] Tg C yr^{-2}) and urban ([-1.00, -0.93] Tg C yr^{-2}) classes. On the other hand, forest gains mainly from shrub and grass conversion resulted in a positive GPP effect (i.e., [1.52, 2.71] Tg C yr^{-2}). Together, net forest change had a significant negative effect on GPP (i.e., [-1.98, -1.39] Tg C

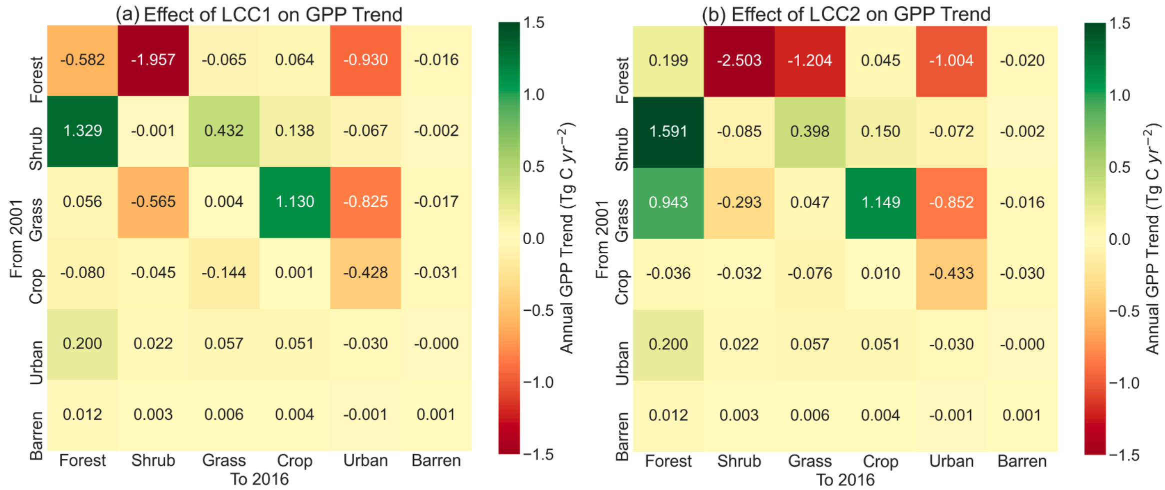

Fig. 3. Effects of land cover change (LCC) on annual GPP trends across LCC types constrained by simulations of LCC1 (a) and LCC2 (b). Model simulations of LCC1 and LCC2 are seen in Table 1. All GPP trends are statistically significant (i.e., P < 0.05) unless labeled by *.

yr^{-2}).

Urban expansion exerted a strong and consistent negative effect on GPP regardless of which type of vegetation was replaced, especially for forest ([-1.00, -0.93] Tg C yr^{-2}), grass ([-0.85, -0.83] Tg C yr^{-2}) and cropland ([-0.43, -0.43] Tg C yr^{-2}) (Fig. 3). Since there was very little loss of urban area, the cumulative net effect of urban change on GPP was even stronger ([-2.03, -1.92] Tg C yr^{-2}) than the net effect of forest change. Crop expansion had a positive effect on GPP ([+1.39, +1.40] Tg C yr^{-2}), mostly from replacement of grass cover (Fig. 3). Overall, the net effect of crop change on GPP was [+0.66, +0.79] Tg C yr^{-2} after considering the negative GPP effect from crop shrinkage. All stable land covers with occasional disturbances showed nonsignificant GPP trends during the study period (i.e., P > 0.05; Fig. 3), which were not involved in the above integration analysis.

3.3. Effects of major land cover change types on GPP by regions

At the regional scale, forest loss (or deforestation) contributed to the largest GPP reductions in the Southeast ([-1.95, -1.35] Tg C yr^{-2}) and Northwest ([-1.57, -0.76] Tg C yr^{-2}) regions (Fig. 4) while forest gains (or reforestation) contributed only minor GPP increases, leading to large net negative effects of forest LCC on GPP in both regions. Urbanization resulted in strong GPP reductions mainly in the Southeast ([-1.04, -1.09] Tg C yr^{-2}) and Midwest ([-0.51, -0.51] Tg C yr^{-2}). Crop expansion enhanced annual GPP trends in all regions, especially in the Midwest ([0.73, 0.78] Tg C yr^{-2}). However, the Midwest was also the region with the largest negative GPP effect due to cropland shrinkage ([-0.32, -0.28] Tg C yr^{-2}) (Fig. 4).

3.4. Comparison of land cover change effect with climate effect on GPP

Annual total GPP over the change area of CONUS showed a large inter-annual variation from 2001 to 2016 (Fig. 5a). Our simulations indicate that LCC explains 22.8% (P < 0.01; LCC1) to 43.2% (P < 0.01; LCC2) of this variation, which is much smaller than climate effects (i.e., 70.5 % (P < 0.01; CLM2) to 73.1% (P < 0.01; CLM1)) (Fig. 5a). However, for the long-term GPP trend, LCC exerted a significant negative effect of −2.22 Tg C yr^{-2} (P < 0.01; LCC1) to −1.83 Tg C yr^{-2}(P < 0.01; LCC2) (Fig. 5b). In contrast, climate change played a minor role in driving the GPP trend, with positive (but not statistically significant) effects of 0.17 Tg C yr^{-2} (P > 0.05; CLM1) to 0.92 Tg C yr^{-2} (P > 0.05; CLM2) (Fig. 5b). Overall, the actual GPP over the change area decreased during the study period (-1.72 Tg C yr^{-2}, P = 0.21), though the trend was not statistically significant due to the high interannual variability of GPP and because the LCC effects on GPP were partially mitigated by climate change effects. Note that, the uncertainty of GPP trends from the incomplete NLCD is marginal and does not change the contrasting effects of LCC and climate change (Fig. 5b).

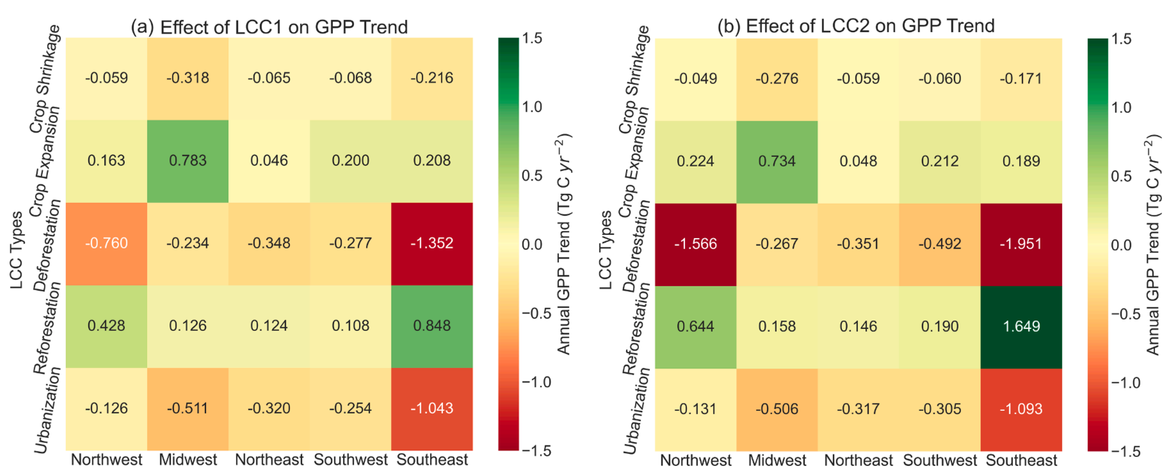

Fig. 4. Effects of major land cover change (LCC) types on annual GPP trends across regions constrained by simulations of LCC1 (a) and LCC2 (b). Model simulations of LCC1 and LCC2 are seen in Table 1. All GPP trends here are statistically significant (i.e., P < 0.05).

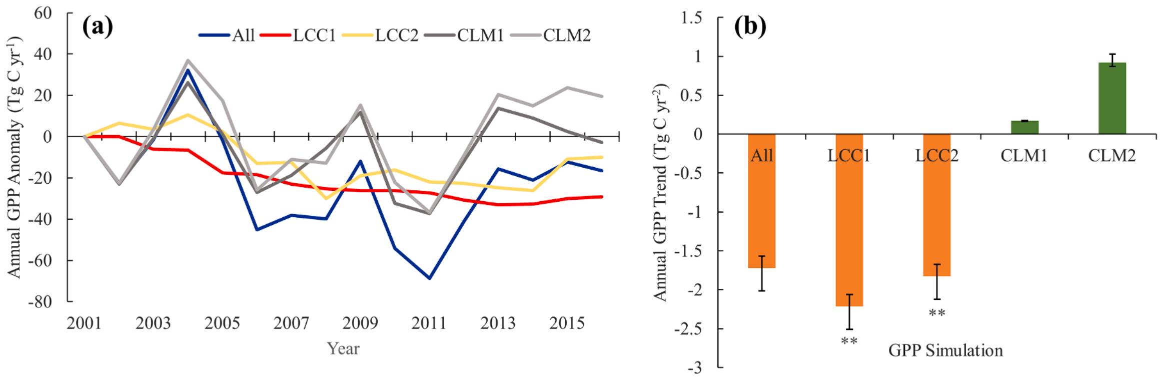

Fig. 5. Effects of land cover change (LCC) and climate change on interannual variations (a) and trends (b) in total GPP over change areas across the CONUS. The anomaly in (a) is relative to the base year of 2001. Model simulations (i.e., LCC1, LCC2, CLM1 and CLM2) are seen in Section 2 and Table 1. The label ** in (b) represents the significance level of annual trend (i.e., P < 0.01). The upper and lower error bars in (b) are from group simulations of "early" LCC and "late" LCC (seen in Section 2.4), respectively.

In most regions (except the Midwest), LCC effects on GPP trends were stronger and more negative than climate effects over the change areas (Figs. 6 & 7). The statistically significant area (i.e., P < 0.05) for LCC effects on GPP (i.e., 51.1% of total change area for LCC2 and 65.7% for LCC1) is much larger than that for climate effects (i.e., 10.6% for CLM1 and 25.8% for CLM2) (Fig. S2). In the Midwest, LCC showed an overall positive GPP effect mainly due to cropland expansion (Figs. 4 & 7). The weak positive climate effect further enhanced the GPP increase over this region. Besides the Midwest, the significant negative LCC effect on GPP in the Northwest and Northeast were also to some degree lessened by weak positive climate effects (Fig. 7). However, in the Southeast and Southwest, weak negative climate effects slightly reinforced negative LCC effects on GPP.

3.5. Evaluation of land cover change effects on GPP from the TRENDY ensemble

During the study period, the TRENDY model ensemble showed a

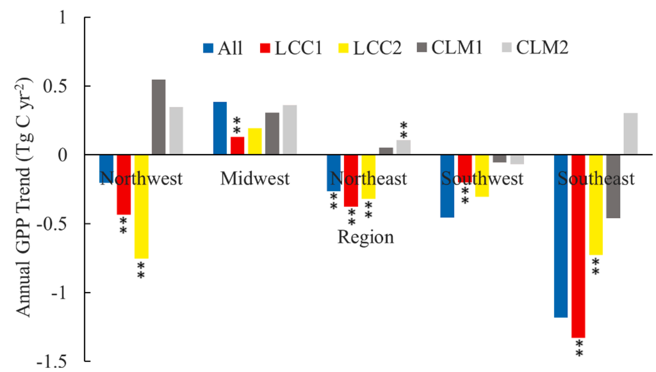

Fig. 7. Effects of land cover change (LCC) and climate change on annual total GPP trends over change areas of different regions in CONUS. The label ** represents the statistical significance level of annual GPP trend (i.e., P < 0.05).

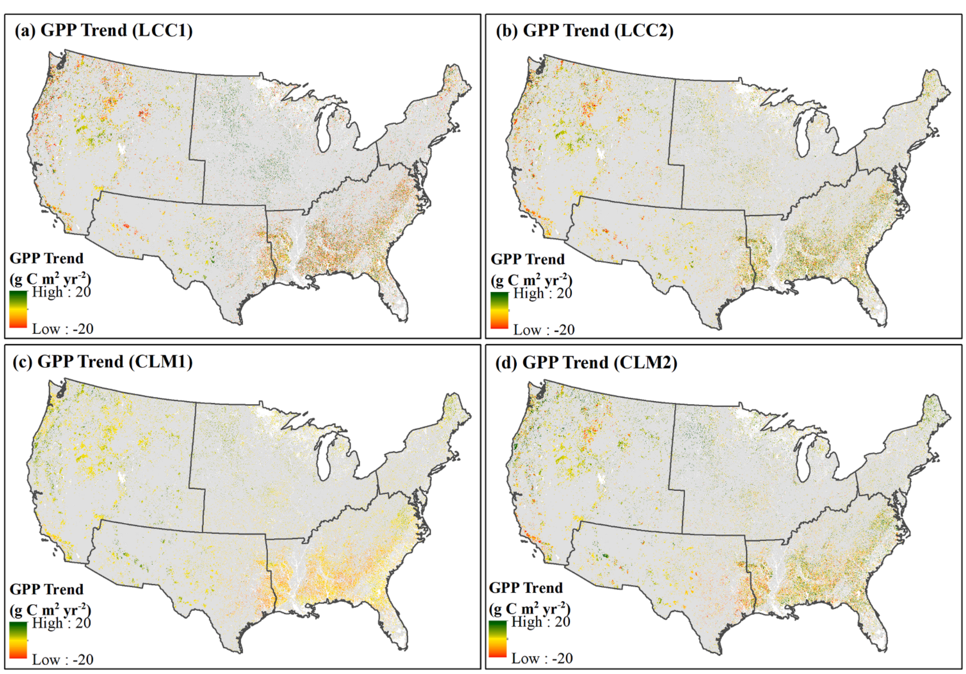

Fig. 6. Spatial patterns of effects of land cover change (LCC) (a, b) and climate change (c, d) on annual GPP trends from 2001 to 2016 over change areas across CONUS, with stable areas (gray), and water/wetland areas (white). Model simulations (i.e., LCC1, LCC2, CLM1 and CLM2) are described in Section 2 and Table 1, and corresponding statistical significances are shown in Fig. S2.

contrasting LCC effect on GPP compared to the CCW (Fig. 8). According to the CCW, LCC had a strong negative effect on annual GPP, with a cumulative change in the range of [-42.3, -30.3] Tg C from 2001 to 2016. However, in ensemble simulations from TRENDY, LCC had a weak positive influence on GPP, with a cumulative GPP change of 3.9 ± 9.0 Tg C over the change area. Among TRENDY models, 5 of 6 showed positive LCC influences with the maximum GPP effect of 20.6 Tg C from JULES (Fig. 8), while the SURFEX model showed a negative influence (i.e., -6.2 Tg C). However, the latter is still out of the value range suggested by the CCW. Our independent simulations based on LUH2 showed similar LCC effect on GPP with a range of [-2.4, 4.9] Tg C based on the coarse NLCD change mask (i.e., 0.25-degree) and a slightly wider range of [-7.1, 15.3] Tg C based on the fine-scale change mask (i.e., 300-m). Despite differences from these two statistical masks, simulated GPP influences from LUH2 based on CCW are comparable with TRENDY ensemble means, suggesting the deficiency of LUH2 may likely be responsible for the underestimation of LCC-induced negative GPP influences in TRENDY.

Based on the wildfire mask from MTBS (Fig. S1), we further compared LCC effects from NLCD and LUH2 on annual GPP trends over fire and non-fire regions (Fig. S4). Interestingly, both NLCD and LUH2 showed larger influences of LCC over non-fire disturbed regions than fire disturbed regions (in terms of the direct LCC effect from LCC1 and indirect LCC effect from LCC2 in Fig. S4), likely due to the relatively smaller fire burning area and post-fire vegetation recovery. However, LUH2 appeared to show relatively equivalent discrepancies with NLCD in LCC effects over fire and non-fire disturbed regions (Fig. S4), which suggests that natural disturbance caused by wildfire is one of the major factors explaining the discrepancy between TRENDY and our NLCD-based simulations.

4. Discussion

4.1. Spatial & temporal patterns of land cover change

Our study highlighted the major patterns of LCC over CONUS based on the most recent NLCD dataset. Excluding changes in water and other wetlands, LCC occurred over 7.9% of the total CONUS area from 2001 to 2016 (Fig. 1), which was mainly characterized by forest loss (10.8% of total change area), crop expansion (9.7% of total change area), and urbanization (4.7% of total change area) (Fig. 2). Currently, debate still exists on the major patterns of LCC over the CONUS. For example, the national inventory data from FAOSTAT shows an increasing trend in total forest area, but a decreasing trend in cropland over the CONUS since 2001 (Fig. S5). The commonly used global harmonized land cover data of LUH2, with a spatial resolution of 0.25 degree and constrained by FAOSTAT, shows similar forest and cropland trends despite more inter-annual fluctuation (Fig. S5). In contrast, remote-sensing based global land cover products such as MODIS (500-m resolution) and ESA-CCI (300-m resolution) show a decrease in forest areas, but no trend or even an increase in croplands (Fig. S5). Our study, based on the most recent NLCD with a nominal resolution of 30 m, presents an opportunity to assess the differences and potentially reconcile the debate on the recent LCC pattern over the CONUS.

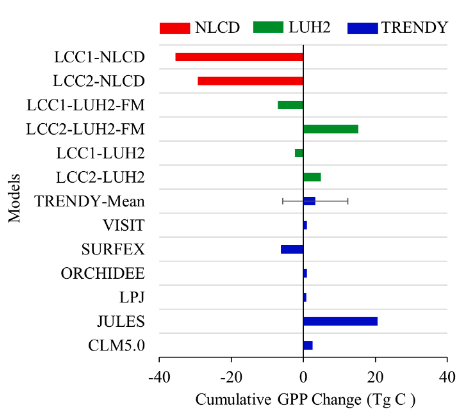

Fig. 8. Comparisons of land cover change (LCC)-induced GPP changes from satellite-derived land cover data (NLCD), the harmonized land use product (LUH2) and TRENDY models over the change area identified by NLCD from 2001 to 2016. LCC-induced GPP trends from NLCD and LUH2 were simulated by CCW and based on model scenarios of LCC1 and LCC2 in Table 1, while LCC influences from all TRENDY models were the differences between S3 and S2 in Table S2. Note that LCC1-NLCD, LCC2-NLCD, LCC1-LUH2-FM and LCC2-LUH2-FM were derived based on the fine-scale land-cover change mask (i.e., 300-m), while other simulations based on the masks with their original coarse spatial resolutions. Annual GPP anomalies for all these model simulations are shown in Fig. S3.

Overall, opposite LCC trends of FAOSTAT/LUH2 with NLCD 2016 reflect the deficiency of these two data sources in characterizing regional LCC signals (Goldewijk et al., 2017; Yu et al., 2019). The coarse spatial resolution of LUH2 and the incomplete spatial representation of FAOSTAT may be ill-equipped to document LCC predominantly occurring at a finer, more localized scale. Another possible reason for these discrepancies is that FAOSTAT/LUH2 focuses on land use, while NLCD mainly focuses on land cover. The difference in land use- and cover-definitions likely contributed to the observed discrepancies (Coulston et al., 2014). For example, timber harvest will not change the land use type of the area as long as the land is not used for some other purposes (e.g., agriculture). Harvested forest land, in contrast, are likely to be identified as non-forest after the harvest based on remotely sensed data. Therefore, a fair portion of forest losses by timber harvest as well as other natural disturbances that are reflected by NLCD may be missing in the FAO/LUH2. In addition, based on an independent high-resolution multisource harmonized national LCC database over the CONUS, Yu et al. (2019) found a striking underestimation of cropland changes in LUH2. Such underestimation was mainly inherited from the national inventory data from FAOSTAT, which largely underestimated crop expansion due to its cropland definition. This uncertainty of cropland change was further propagated to the modeled forest change in LUH2 (Goldewijk et al., 2017; Yu et al., 2019). Remote sensing-based global land cover products are more consistent with NLCD 2016 than FAOSTAT/LUH2, but the MODIS land cover product showed higher biases in absolute areas for different land covers, especially for forests and shrublands, while ESA-CCI showed less interannual variation than NLCD 2016 (Fig. S5). Such discrepancies could result from differences in land cover/type definition, classification strategies, and remote sensing data with varying spatial/temporal resolutions and spectral characteristics (Li et al., 2018; Sulla-Menashe et al., 2019).

The NLCD 2016 reveals several key characteristics of LCC across the CONUS. For example, forest loss was mainly associated with conversion to grass and shrubland during the study period (Fig. 2), which differs from tropical deforestation that is mainly linked to cropland expansion (Barraclough, 2013; Pendrill et al., 2019). The Southeast and Northwest are the two major regions affected by deforestation in the CONUS (Fig. 2), which were largely driven by timber harvesting, fire and mortality from drought and insect outbreaks (Williams et al., 2010; Curtis et al., 2018; Howard & Liang, 2019; Homer et al., 2020). Cropland expansion mostly occurred at the expense of grassland, mostly in the Midwest, which is consistent with previous research (Wright & Wimberly, 2013; Yu & Lu, 2018). Urbanization, occurring most prominently in the Southeast, was largely linked to grassland and forest losses (Fig. 2). These transitions differed from other countries with urbanization mainly at the cost of cropland (d`Amour et al., 2017; van Vliet et al., 2017). During the study period, the rate of forest loss tended to slow down after 2011 (Fig. 1d), which is generally consistent with national industrial timber markets (Howard & Liang, 2019; Homer et al., 2020). A similar temporal pattern was also observed for urbanization (Fig. 1d), which was possibly linked to the 2008 global economic recession (Homer et al., 2020).

4.2. Decoupling effects of land cover change on GPP from climate change

LCC induced by anthropogenic activity and natural disturbances have profound impacts on terrestrial GPP. However, such influences are usually aggregated with other environmental factors, such as climate, and empirically disentangling their effects is still a challenge. In this study, we decoupled the effects of LCC and climate change on terrestrial carbon sequestration based on a remote sensing-based ecosystem model and newly released high-quality land cover data. Through designed model simulations, we narrowed down the effect of LCC on recent GPP changes over the CONUS to a specific range on the top of the influence of climate change/variability.

From 2001-2016, we observed a strong negative effect on GPP from deforestation in the CONUS (i.e., [-4.69, -2.90] Tg C yr^{-2}), especially in the Southeast ([-1.95, -1.35] Tg C yr^{-2}) and Northwest ([-1.57, -0.76] Tg C yr^{-2}). Although reforestation positively affected GPP (i.e., [1.52, 2.71] Tg C yr^{-2}), it did not completely offset the negative effects of deforestation, resulting in an overall net negative GPP trend by forest cover change over the CONUS (Figs. 3 & 4). Forests are the key biome in maintaining ecosystem functions and serve as a major contributor in land carbon sequestration (Domke et al., 2020; Woodbury et al., 2007). Previous studies in China showed that the national-scale forest afforestation/reforestation programs since 2000 have promoted substantial vegetation productivity (Zhang et al., 2014; Chen et al., 2021). Here, the contrasting picture over the CONUS reveals a worrisome trend on the recent decline of GPP related to forest change. Depending on the specific mechanisms driving deforestation in different regions (e.g., Southeast mainly related to timber harvest and Northwest mainly related to fire) (Fig. S1; Harris et al., 2016; Curtis et al., 2018), active forest management—such as fire management, timber harvest control, shifting to non-timber forest products or tree planting—could be useful in mitigating the negative effects on GPP from forest change (Noormets et al., 2015; Domke et al., 2020). However, some federal forest management rules may not be applicable to privately-owned forests. For example, the forests of the Southeast are predominantly privately-owned (Wear & Greis, 2002) and timber harvesting contributes significantly to deforestation in this region. Nevertheless, it worth pointing out that deforestation related to temporal disturbances (e.g., timber harvest and wildfires) could strong reduce ecosystem GPP immediately, but its negative effect can be gradually offset by post-disturbance vegetation recovery (Fig. S4; Gitas et al., 2012). The long-term effects of deforestation at the regional scale are determined by the tradeoff between the disturbance frequency and vegetation recovery time.

Compared with forests, urbanization affected a much smaller area (Fig. 2), but the net effects on GPP were disproportionally high ([-2.03, -1.92] Tg C yr^{-2}), and even stronger than net forest cover changes due to the cumulative and direct effects of removing all vegetation (Fig. 3). The Southeast ([-1.04, -1.09] Tg C yr^{-2}) and Midwest ([-0.51, -0.51] Tg C yr^{-2}) were the two major regions associated with strong GPP reductions caused by urbanization (Fig. 3). Our findings on the substantial effect of urbanization on GPP is generally consistent with previous vegetation productivity studies (Liu et al., 2019; Li et al., 2020). However, due to the treatment of urban areas as a homogenous surface without plants, the impact of urbanization on GPP in our study may be overestimated (Guan et al., 2019).

Unlike forest and urban changes, the net change in croplands showed an overall positive effect on GPP (i.e., [+0.66, +0.79] Tg C yr^{-2}). Crop expansion occurring primarily at the cost of grasslands was a major contributor to GPP ([+1.39, +1.40] Tg C yr^{-2}) over the study period. Due to crop expansion, the Midwest became the only region with an overall positive LCC effect on GPP (Figs. 6 & 7). Croplands tend to be more productive than other natural vegetation (e.g., grasslands) due to human management (e.g., irrigation, fertilization, selection of productive cultivars; Licker et al., 2010), resulting in a positive net effect on GPP. However, due to the exceptionally high turnover rate of carbon in crop systems (e.g., linked with harvest and consumption), croplands have limited potential in carbon storage when compared with natural vegetation (Wolf et al., 2015). Therefore, crop expansion, even if it increases GPP and net primary production, would likely have less effect on the land carbon sink, and thus less potential to mitigate the ongoing global warming (Bajželj et al., 2014; Zhang et al., 2019). In addition, widespread crop expansion in the Midwest at the cost of grasslands has threatened biodiversity in this region (Wright & Wimberly, 2013; Lark et al., 2015, 2020).

Altogether, our study shows a strong negative influence of LCC on annual GPP over the CONUS (i.e., [-2.6, -1.9] Tg C yr^{-2}), which outweighs the slight positive GPP trends from climate (i.e., [0.17, 0.92] Tg C yr^{-2}). However, climate did play a major role in determining interannual variation of GPP over the change area (Fig. 5). Theoretically, the influence of LCC on GPP will diminish or even flatten with time due to post-disturbance recovery/succession (Lambin et al., 2001; Wang et al., 2020). During this period, climate will either enhance or delay this process along with other environmental and human factors. In this study, we showed the spatial pattern of climate influences on GPP by overlaying the effect of LCC (Figs. 6 & 7). Overall, climate change/-variability alleviated negative LCC effects in the northern CONUS but worsened their effects in the southern CONUS (Fig. 6) largely due to droughts (Berdanier & Clark, 2016; Park Williams et al., 2017). Our efforts in decoupling the effects of LCC and climate change on GPP can help enhance our understanding of recent carbon dynamics related to human and natural disturbances over the CONUS.

4.3. Performance of TRENDY ensemble simulations

Based on the long-term LUH2 global harmonized land use data, land surface models from the TRENDY ensemble provide estimates of the influence of LCC at both the global and regional scales (Sitch et al., 2015; Quéré et al., 2018;). However, our evaluation showed that none of the selected models captured the strong negative GPP effects over the CONUS (Fig. 8). On the contrary, 5 of 6 models simulated positive LCC effects on GPP. Our simulations based on the CCW (Fig. 8) further suggest that these discrepancies were likely caused by the uncertainty in the LUH2 dataset (Goldewijk et al., 2017; Yu et al., 2019), which shows opposite trends of forest and cropland areas over the CONUS when compared with finer-resolution remote sensing products (Fig. S5). Previous studies have shown that carbon emissions from LCC over the CONUS have been largely underestimated due to the mischaracterization of crop and forest changes (Yu & Lu, 2018; Yu et al., 2019). Our study suggests that ignoring the strong GPP reductions caused by LCC might be a key reason for the overestimation of land carbon sink over the CONUS (Liu et al., 2020). Given that TRENDY ensemble simulations provide much of the basis for the Global Carbon Budget (Quéré et al., 2018; Friedlingstein et al., 2019), which show large uncertainties in LCC-induced carbon flux, our study provides evidence for a source of uncertainties in global carbon balance, to which much more attention needs to be paid. However, discrepancies between TRENDY and our CCW simulations could be related to other factors, such as model structures (process-based models for TRENDY vs. a light-use efficiency model for CCW), model implementations of LCC effects (land-use change and management practices in TRENDY vs. land cover change in CCW), and differences in climate inputs (global climate data for TRENDY vs. regional climate data for CCW) (Bastos et al. 2020). These potential factors are not strictly quantified in our study but are worthy of future investigation.

4.4. Implications & uncertainties

Reducing anthropogenic carbon emissions is a critical mechanism for mitigating global warming below a secure threshold, which is an urgent yet challenging task (Rogelj et al., 2016). The actions through conservation, restoration and improved land management are cost-effective ways or “natural climate solutions” to global warming mitigation

(Griscom et al., 2017). Currently, a series of “natural climate solutions” on natural and agricultural lands are being evaluated to sustain the U.S. terrestrial carbon sink and meet Paris Agreement carbon targets (Fargione et al., 2018). Among them, reforestation, natural forest management and preservation of grassland show the highest climate mitigation potential, especially when carbon storage is highly valued (Fargione et al., 2018). However, according to our study based on the newest NLCD database, the recent LCC trend since 2001 (characterized by net forest loss, cropland expansion from grassland, and urban expansion from forest and grassland; Fig. 2) appears to departure from these initiatives. How to account for the past LCC trajectory and the weakened carbon sequestration capacity identified by this study is critical in implementing natural climate solutions, for example in the establishment of baseline trends (Roe et al., 2019; Anderegg et al., 2020).

In this study, we comprehensively examined the spatially detailed and regionally aggregated LCCs and their impacts on vegetation productivity over the CONUS. Currently, it is still a challenge to effectively disaggregate LCC effect on GPP from climate change/variability effect. Based on a remote sensing-driven ecosystem model and scenario simulations, we teased out the respective effect of LCC and climate change on GPP in specific ranges rather a definite quantity, which we believe to be more reasonable than previous modeling studies (Zhang et al., 2014; Sun et al., 2018). However, it is worth noting that simulations for LCC (i.e., LCC2) and climate (i.e., CLM2) alone may have confounding effects from each other and potentially other factors (e.g., regrowth, CO_2 fertilization, land management etc.) that are confounded the signal of canopy greenness, and hard to separate under our current modeling scheme. Combining our remote-sensing constrained estimates and process-based models with localized high-quality LCC inputs is a promising way to better understand LCC-induced carbon dynamics. In addition, wetlands were excluded in our study given our focus on terrestrial ecosystems. Although total wetlands increased over a relatively small area (i.e., 0.09% of total CONUS area) (Homer et al., 2020), conversions between wetlands and other vegetation types, and among wetlands themselves (e.g., herbaceous vs. woody) may still exert a significant GPP control, which is worthy of future exploration. Third, our study focused on a relatively short period from 2001 to 2016 due to the temporal constraint of the NLCD records. With updates of more consistent historic (i.e., before 2000) and higher frequency (e.g., from 2~3 years to yearly/sub-yearly) NLCD in the future, LCC influences on GPP could be further refined and re-evaluated particularly at the regional scale. Lastly, our study is focused on GPP, a primary control on the net carbon exchange (NEE). However, NEE is further constrained by ecosystem respiration (i.e., autotrophic and heterotrophic) (Chapin et al., 2006). How LCC influences the ecosystem respiration and net land carbon balance over the CONUS is an interesting topic, which is worthy of exploration in the future.

5. Conclusions

Based on NLCD 2016 and a remote-sensing driven ecosystem model run on the GEE cloud platform, we explored the effect of land cover change (LCC) on GPP over the conterminous U.S. from 2001 to 2016. During the study period, forest loss, cropland expansion, and urbanization dominated LCC patterns. Our model simulations estimated the net effect of forest changes on total GPP was [-1.98, -1.39] Tg C yr^{-2}, followed by urban change ([-2.03, -1.92] Tg C yr^{-2}) and crop change ([+0.66, +0.79] Tg C yr^{-2}). Regionally, the Southeast contributed the largest GPP reduction due to deforestation (-1.95, -1.35] Tg C yr^{-2}), followed by the Northwest ([-1.57, -0.76] Tg C yr^{-2}), while the Midwest contributed largest GPP increase related to crop expansion ([0.73, 0.78] Tg C yr^{-2}), and the Southeast contributed the largest GPP reduction related to urbanization ([-1.0, -1.1] Tg C yr^{-2}). Overall, LCC led to a strong negative trend on total GPP over the CONUS ([-2.2, -1.8] Tg C yr^{-2}), while climate change had a relatively small positive effect (but not statistically significant) over the LCC area ([0.17, 0.92] Tg yr^{-1}) during the study period. Ensemble simulations from TRENDY did not capture the strong negative effects of LCC on GPP, likely due to the deficiency of the adopted land use/cover data. Our study demonstrates that recent LCC appears to reduce the carbon sequestration capacity of the land surface across the CONUS in ways that are not particularly well-represented in land surface models. Such a novel perspective on LCC-induced GPP changes could enhance our understanding of ecosystem function changes and carbon dynamics under the background of anthropogenic activity and climate change.

Declaration of Competing Interest

The authors declare that they have no known competing financial interests or personal relationships that could have appeared to influence the work reported in this paper.

Acknowledgements

We acknowledge USGS for providing NLCD 2016 data, NASA Science Teams for providing MODIS VI products and Daymet V3 climate data, Dr. Stephen Sitch from University of Exeter and Dynamic Global Vegetation Model Project team for providing TRENDY V7 data, and Earth Engine platform provided by Google. This study is supported by NASA Carbon Cycle Science (NNX17AE69G). J. Mao was supported by the Terrestrial Ecosystem Science Scientific Focus Area (TESSFA) project funded by the US Department of Energy, Office of Science, Office of Biological and Environmental Research. Oak Ridge National Laboratory is managed by UT-Battelle, LLC, for the DOE under contract DE-AC05-100-00OR22725. The authors declare no conflict of interests.

Supplementary materials

Supplementary material associated with this article can be found, in the online version, at doi:10.1016/j.agrformet.2021.108609.

References

Allen, R.G., Pereira, L.S., Raes, D., Smith, M., 1998. Crop evapotranspiration-Guidelines for computing crop water requirements-FAO Irrigation and drainage paper 56. Fao, Rome 300 (9), D05109.
Anav, A., Friedlingstein, P., Beer, C., Ciais, P., Harper, A., Jones, C., Murray-Tortarolo, G., Papale, D., Parazoo, N.C., Peylin, P., 2015. Spatiotemporal patterns of terrestrial gross primary production: A review. Rev. Geophys. 53 (3), 785–818.
Anderegg, W.R., Trugman, A.T., Badgley, G., Anderson, C.M., Bartuska, A., Ciais, P., Cullenward, D., Field, C.B., Freeman, J., Goetz, S.J., 2020. Climate-driven risks to the climate mitigation potential of forests. Science 368 (6497).
Arneth, A., Sitch, S., Pongratz, J., Stocker, B.D., Ciais, P., Poulter, B., Bayer, A.D., Bondeau, A., Calle, L., Chini, L.P., Gasser, T., Fader, M., Friedlingstein, P., Kato, E., Li, W., Lindeskog, M., Nabel, J.E.M.S., Pugh, T.A.M., Robertson, E., Zaehle, S., 2017. Historical carbon dioxide emissions caused by land-use changes are possibly larger than assumed. Nat. Geosci. 10 (2), 79–84. https://doi.org/10.1038/ngeo2882.
Bajželj, B., Richards, K.S., Allwood, J.M., Smith, P., Dennis, J.S., Curmi, E., Gilligan, C.A., 2014. Importance of food-demand management for climate mitigation. Nature Climate Change 4 (10), 924–929.
Barraclough, S.L., 2013. Agricultural expansion and tropical deforestation: International trade, poverty and land use. Routledge.
Bastos, A., O'Sullivan, M., Ciais, P., Makowski, D., Sitch, S., Friedlingstein, P., Chevallier, F., Rödenbeck, C., Pongratz, J., Luijkx, I.T., 2020. Sources of uncertainty in regional and global terrestrial CO2 exchange estimates. Glob. Biogeochem. Cycles 34 (2), e2019GB006393.
Beer, C., Reichstein, M., Tomelleri, E., Ciais, P., Jung, M., Carvalhais, N., Rödenbeck, C., Arain, M.A., Baldocchi, D., Bonan, G.B., 2010. Terrestrial gross carbon dioxide uptake: Global distribution and covariation with climate. Science 329 (5993), 834–838.
Berdanier, A.B., Clark, J.S., 2016. Multiyear drought-induced morbidity preceding tree death in southeastern US forests. Ecol. Appl. 26 (1), 17–23.
Chapin, F.S., Woodwell, G.M., Randerson, J.T., Rastetter, E.B., Lovett, G.M., Baldocchi, D.D., Clark, D.A., Harmon, M.E., Schimel, D.S., Valentini, R., 2006. Reconciling carbon-cycle concepts, terminology, and methods. Ecosystems 9 (7), 1041–1050.
Chen, J., Chen, J., Liao, A., Cao, X., Chen, L., Chen, X., He, C., Han, G., Peng, S., Lu, M., 2015. Global land cover mapping at 30 m resolution: A POK-based operational approach. ISPRS J. Photogramm. Remote Sens. 103, 7–27.
Chen, S., Zhang, Y., Wu, Q., Liu, S., Song, C., Xiao, J., Band, L.E., Vose, J.M., 2021. Vegetation structural change and CO2 fertilization more than offset gross primary

production decline caused by reduced solar radiation in China. Agric. For. Meteorol. 296, 108207 https://doi.org/10.1016/j.agrformet.2020.108207.
Coulston, J.W., Reams, G.A., Wear, D.N., Brewer, C.K., 2014. An analysis of forest land use, forest land cover and change at policy-relevant scales. Forestry 87 (2), 267–276.
Coulston, J.W., Wear, D.N., Vose, J.M., 2015. Complex forest dynamics indicate potential for slowing carbon accumulation in the southeastern United States. Sci. Rep. 5, 8002.
Curtis, P.G., Slay, C.M., Harris, N.L., Tyukavina, A., Hansen, M.C., 2018. Classifying drivers of global forest loss. Science 361 (6407), 1108–1111. https://doi.org/10.1126/science.aau3445.
d'Amour, C.B., Reitsma, F., Baiocchi, G., Barthel, S., Güneralp, B., Erb, K.-H., Haberl, H., Creutzig, F., Seto, K.C., 2017. Future urban land expansion and implications for global croplands. Proc. Natl. Acad. Sci. 114 (34), 8939–8944.
Danielson, J.J., Gesch, D.B., 2011. Global multi-resolution terrain elevation data 2010 (GMTED2010). US Department of the Interior, US Geological Survey.
Dannenberg, M.P, Song, C., Hakkenberg, C.R., 2018. A long-term, consistent land cover database for the southeastern United States using Automatic Adaptive Signature Generalization (AASG). Photogrammetric Eng. Remote Sensing 84 (9), 559–568.
Didan, K., Munoz, A.B., Solano, R., Huete, A., 2015. MODIS vegetation index user's guide (MOD13 series). University of Arizona: Vegetation Index and Phenology Lab.
Domke, G.M., Oswalt, S.N., Walters, B.F., Morin, R.S., 2020. Tree planting has the potential to increase carbon sequestration capacity of forests in the United States. Proc. Natl. Acad. Sci. 117 (40), 24649–24651.
Erb, K.-H., Kastner, T., Luyssaert, S., Houghton, R.A., Kuemmerle, T., Olofsson, P., Haberl, H., 2013. Bias in the attribution of forest carbon sinks. Nature Climate Change 3 (10), 854–856. https://doi.org/10.1038/nclimate2004.
ESA. (2017). *Land cover CCI product user guide version 2*.
Falkowski, P., Scholes, R.J., Boyle, E.E.A., Canadell, J., Canfield, D., Elser, J., Gruber, N., Hibbard, K., Högberg, P., Linder, S., 2000. The global carbon cycle: A test of our knowledge of earth as a system. Science 290 (5490), 291–296.
Fargione, J.E., Bassett, S., Boucher, T., Bridgham, S.D., Conant, R.T., Cook-Patton, S.C., Ellis, P.W., Falcucci, A., Fourqurean, J.W., Gopalakrishna, T., 2018. Natural climate solutions for the United States. Sci. Adv. 4 (11), eaat1869.
Foley, J.A., 2005. Global Consequences of Land Use. Science 309 (5734), 570–574. https://doi.org/10.1126/science.1111772.
Friedlingstein, P., Jones, M., O'sullivan, M., Andrew, R., Hauck, J., Peters, G., Peters, W., Pongratz, J., Sitch, S., Le Quéré, C., 2019. Global carbon budget 2019. Earth Sys. Sci. Data 11 (4), 1783–1838.
Frolking, S., Palace, M.W., Clark, D.B., Chambers, J.Q., Shugart, H.H., Hurtt, G.C., 2009. Forest disturbance and recovery: A general review in the context of spaceborne remote sensing of impacts on aboveground biomass and canopy structure. J. Geophys. Res. 114 (G2).
Fry, J.A., Coan, M.J., Homer, C.G., Meyer, D.K., Wickham, J.D., 2008. Completion of the National Land Cover Database (NLCD) 1992–2001 land cover change retrofit product. US Geological Survey Open-File Rep. 1379, 18.
Gitas, I., Mitri, G., Veraverbeke, S., Polychronaki, A., 2012. Advances in Remote Sensing of Post-Fire Vegetation Recovery Monitoring—A Review. In: Fatoyinbo, L. (Ed.), Remote Sensing of Biomass—Principles and Applications. InTech. https://doi.org/10.5772/20571.
Gorelick, N., Hancher, M., Dixon, M., Ilyushchenko, S., Thau, D., Moore, R., 2017. Google Earth Engine: Planetary-scale geospatial analysis for everyone. Remote Sens. Environ. 202, 18–27.
Griscom, B.W., Adams, J., Ellis, P.W., Houghton, R.A., Lomax, G., Miteva, D.A., Schlesinger, W.H., Shoch, D., Siikamäki, J.V., Smith, P., 2017. Natural climate solutions. Proc. Natl. Acad. Sci. 114 (44), 11645–11650.
Guan, X., Shen, H., Li, X., Gan, W., Zhang, L., 2019. A long-term and comprehensive assessment of the urbanization-induced impacts on vegetation net primary productivity. Sci. Total Environ. 669, 342–352.
Hansen, M.C., Potapov, P.V., Moore, R., Hancher, M., Turubanova, S.A., Tyukavina, A., Thau, D., Stehman, S.V., Goetz, S.J., Loveland, T.R., 2013. High-resolution global maps of 21st-century forest cover change. Science 342 (6160), 850–853.
Hansis, E., Davis, S.J., Pongratz, J., 2015. Relevance of methodological choices for accounting of land use change carbon fluxes. Glob. Biogeochem. Cycles 29 (8), 1230–1246. https://doi.org/10.1002/2014GB004997.
Harris, N.L., Hagen, S.C., Saatchi, S.S., Pearson, T.R.H., Woodall, C.W., Domke, G.M., Braswell, B.H., Walters, B.F., Brown, S., Salas, W., Fore, A., Yu, Y., 2016. Attribution of net carbon change by disturbance type across forest lands of the conterminous United States. Carbon Balance Manage. 11 (1), 24. https://doi.org/10.1186/s13021-016-0066-5.
Harris, Nancy L., Gibbs, D.A., Baccini, A., Birdsey, R.A., de Bruin, S., Farina, M., Fatoyinbo, L., Hansen, M.C., Herold, M., Houghton, R.A., Potapov, P.V., Suarez, D. R., Roman-Cuesta, R.M., Saatchi, S.S., Slay, C.M., Turubanova, S.A., Tyukavina, A., 2021. Global maps of twenty-first century forest carbon fluxes. Nature Climate Change 11 (3), 234–240. https://doi.org/10.1038/s41558-020-00976-6.
Homer, C., Dewitz, J., Yang, L., Jin, S., Danielson, P., Xian, G., Coulston, J., Herold, N., Wickham, J., Megown, K., 2015. Completion of the 2011 National Land Cover Database for the conterminous United States–representing a decade of land cover change information. Photogrammetric Engineering & Remote Sensing 81 (5), 345–354.
Homer, C., Dewitz, J., Jin, S., Xian, G., Costello, C., Danielson, P., Gass, L., Funk, M., Wickham, J., Stehman, S., Auch, R., Riitters, K., 2020. Conterminous United States land cover change patterns 2001–2016 from the 2016 National Land Cover Database. ISPRS J. Photogramm. Remote Sens. 162, 184–199. https://doi.org/10.1016/j.isprsjprs.2020.02.019.
Houghton, R.A., House, J.I., Pongratz, J., van der Werf, G.R., DeFries, R.S., Hansen, M.C., Le Quéré, C., Ramankutty, N., 2012. Carbon emissions from land use and land-cover change. Biogeosciences 9 (12), 5125–5142. https://doi.org/10.5194/bg-9-5125-2012.
Howard, J.L., Liang, S., 2019. US timber production, trade, consumption, and price statistics, 1965-2017. *Res. Pap. FPL-RP-701*, 701. US Department of Agriculture, Forest Service, Forest Products Laboratory: 1-106, Madison, WI, pp. 1–106.
Hurtt, G., Chini, L., Sahajpal, R., Frolking, S., Bodirsky, B.L., Calvin, K., Doelman, J., Fisk, J., Fujimori, S., Goldewijk, K.K., 2017. Harmonization of global land use scenarios (LUH2): Historical v2. 1h. Earth Sys. Grid Federation.
Jin, S., Homer, C., Yang, L., Danielson, P., Dewitz, J., Li, C., Zhu, Z., Xian, G., Howard, D., 2019. Overall Methodology Design for the United States National Land Cover Database 2016 Products. Remote Sensing 11 (24), 2971. https://doi.org/10.3390/rs11242971.
Goldewijk, K., Beusen, A., Doelman, J., Stehfest, E., 2017. Anthropogenic land use estimates for the Holocene – HYDE 3.2. Earth Sys. Sci. Data 9 (2), 927–953.
Lambin, E.F., Turner, B.L., Geist, H.J., Agbola, S.B., Angelsen, A., Bruce, J.W., Coomes, O.T., Dirzo, R., Fischer, G., Folke, C., 2001. The causes of land-use and land-cover change: Moving beyond the myths. Global Environ. Change 11 (4), 261–269.
Lark, T.J., Meghan Salmon, J., Gibbs, H.K, 2015. Cropland expansion outpaces agricultural and biofuel policies in the United States. Environ. Res. Lett. 10 (4), 044003 https://doi.org/10.1088/1748-9326/10/4/044003.
Lark, T.J., Spawn, S.A., Bougie, M., Gibbs, H.K., 2020. Cropland expansion in the United States produces marginal yields at high costs to wildlife. Nat. Commun. 11 (1), 4295. https://doi.org/10.1038/s41467-020-18045-z.
Le Quéré, C., Andrew, R.M., Friedlingstein, P., Sitch, S., Hauck, J., Pongratz, J., Pickers, P.A., Korsbakken, J.I., Peters, G.P., Canadell, J.G, 2018. Global carbon budget 2018. Earth Sys. Sci. Data 10 (4), 2141–2194.
Li, W., MacBean, N., Ciais, P., Defourny, P., Lamarche, C., Bontemps, S., Houghton, R.A., Peng, S., 2018. Gross and net land cover changes in the main plant functional types derived from the annual ESA CCI land cover maps (1992–2015). Earth Sys. Sci. Data 10 (1), 219–234. https://doi.org/10.5194/essd-10-219-2018.
Li, C., Sun, G., Cohen, E., Zhang, Y., Xiao, J., McNulty, S.G., Meentemeyer, R.K., 2020. Modeling the impacts of urbanization on watershed-scale gross primary productivity and tradeoffs with water yield across the conterminous United States. J. Hydrol. 583, 124581.
Licker, R., Johnston, M., Foley, J.A., Barford, C., Kucharik, C.J., Monfreda, C., Ramankutty, N., 2010. Mind the gap: How do climate and agricultural management explain the 'yield gap'of croplands around the world? Global Ecol. Biogeogr. 19 (6), 769–782.
Liu, X., Pei, F., Wen, Y., Li, X., Wang, S., Wu, C., Cai, Y., Wu, J., Chen, J., Feng, K., 2019. Global urban expansion offsets climate-driven increases in terrestrial net primary productivity. Nat. Commun. 10 (1), 1–8.
Liu, J., Sleeter, B.M., Zhu, Z., Loveland, T.R., Sohl, T., Howard, S.M., Key, C.H., Hawbaker, T., Liu, S., Reed, B., Cochrane, M.A., Heath, L.S., Jiang, H., Price, D.T., Chen, J.M., Zhou, D., Bliss, N.B., Wilson, T., Sherba, J., Poulter, B., 2020. Critical land change information enhances the understanding of carbon balance in the United States. Global Change Biol. 26 (7), 3920–3929. https://doi.org/10.1111/gcb.15079.
Noormets, A., Epron, D., Domec, J.C., McNulty, S.G., Fox, T., Sun, G., King, J.S., 2015. Effects of forest management on productivity and carbon sequestration: A review and hypothesis. Forest Ecol. Manag. 355, 124–140. https://doi.org/10.1016/j.foreco.2015.05.019.
Obermeier, W.A., Nabel, J.E., Loughran, T., Hartung, K., Bastos, A., Havermann, F., Anthoni, P., Arneth, A., Goll, D.S., Lienert, S., Lombardozzi, D., 2021. Modelled land use and land cover change emissions–a spatio-temporal comparison of different approaches. Earth System Dynamics 12 (2), 635–670. https://doi.org/10.5194/esd-12-635-2021.
Pendrill, F., Persson, U.M., Godar, J., Kastner, T., Moran, D., Schmidt, S., Wood, R., 2019. Agricultural and forestry trade drives large share of tropical deforestation emissions. Global Environ. Change 56, 1–10.
Piao, S., Wang, X., Wang, K., Li, X., Bastos, A., Canadell, J.G., Ciais, P., Friedlingstein, P., Sitch, S., 2020. Interannual variation of terrestrial carbon cycle: Issues and perspectives. Global Change Biol. 26 (1), 300–318.
Pielke, R.A., 2005. Land use and climate change. Science 310 (5754), 1625–1626.
Pongratz, J., Reick, C.H., Houghton, R.A., House, J.I., 2014. Terminology as a key uncertainty in net land use and land cover change carbon flux estimates. Earth System Dynamics 5 (1), 177–195. https://doi.org/10.5194/esd-5-177-2014.
Quéré, C., Andrew, R.M., Friedlingstein, P., Sitch, S., Hauck, J., Pongratz, J., Pickers, P. A., Korsbakken, J.I., Peters, G.P., Canadell, J.G., Arneth, A., 2018. Global carbon budget 2018. Earth System Science Data 10 (4), 2141–2194.
Roe, S., Streck, C., Obersteiner, M., Frank, S., Griscom, B., Drouet, L., Fricko, O., Gusti, M., Harris, N., Hasegawa, T., 2019. Contribution of the land sector to a 1.5 C world. Nature Climate Change 1–12.
Rogelj, J., Den Elzen, M., Höhne, N., Fransen, T., Fekete, H., Winkler, H., Schaeffer, R., Sha, F., Riahi, K., Meinshausen, M., 2016. Paris Agreement climate proposals need a boost to keep warming well below 2 C. Nature 534 (7609), 631–639.
Sims, D.A., Rahman, A.F., Cordova, V.D., Baldocchi, D.D., Flanagan, L.B., Goldstein, A. H., Hollinger, D.Y., Misson, L., Monson, R.K., Schmid, H.P., 2005. Midday values of gross CO2 flux and light use efficiency during satellite overpasses can be used to directly estimate eight-day mean flux. Agric. For. Meteorol. 131 (1–2), 1–12.
Sitch, S., Friedlingstein, P., Gruber, N., Jones, S.D., Murray-Tortarolo, G., Ahlström, A., Doney, S.C., Graven, H., Heinze, C., Huntingford, C., Levis, S., Levy, P.E., Lomas, M., Poulter, B., Viovy, N., Zaehle, S., Zeng, N., Arneth, A., Bonan, G., Myneni, R., 2015. Recent trends and drivers of regional sources and sinks of carbon dioxide. Biogeosciences 12 (3), 653–679. https://doi.org/10.5194/bg-12-653-2015.
Sleeter, B.M., Sohl, T.L., Loveland, T.R., Auch, R.F., Acevedo, W., Drummond, M.A., Sayler, K.L., Stehman, S.V., 2013. Land-cover change in the conterminous United

States from 1973 to 2000. Global Environ. Change 23 (4), 733–748. https://doi.org/10.1016/j.gloenvcha.2013.03.006.
Song, C., Chen, J.M., Hwang, T., Gonsamo, A., Croft, H., Zhang, Q., Dannenberg, M., Zhang, Y., Hakkenberg, C., Li, J., 2015. Ecological characterization of vegetation using multisensor remote sensing in the solar reflective spectrum. Remote Sensing Handbook 2, 533–575.
Sulla-Menashe, D., Gray, J.M., Abercrombie, S.P., Friedl, M.A., 2019. Hierarchical mapping of annual global land cover 2001 to present: The MODIS Collection 6 Land Cover product. Remote Sens. Environ. 222, 183–194.
Sun, Z., Wang, X., Yamamoto, H., Tani, H., Zhong, G., Yin, S., Guo, E., 2018. Spatial pattern of GPP variations in terrestrial ecosystems and its drivers: Climatic factors, CO2 concentration and land-cover change, 1982–2015. Ecological Informatics 46, 156–165.
Tamiminia, H., Salehi, B., Mahdianpari, M., Quackenbush, L., Adeli, S., Brisco, B., 2020. Google Earth Engine for geo-big data applications: A meta-analysis and systematic review. ISPRS J. Photogramm. Remote Sens. 164, 152–170.
Thornton, P.E., Thornton, M.M., Mayer, B.W., Wei, Y., Devarakonda, R.S., Vose, R.S., Cook, R.B., 2017. Daymet: Daily Surface Weather Data on a 1-km Grid for North America. Version 3 ORNL DAAC Oak Ridge Tenn, USA.
van Vliet, J., Eitelberg, D.A., Verburg, P.H., 2017. A global analysis of land take in cropland areas and production displacement from urbanization. Global Environ. Change 43, 107–115.
Wang, J.A., Sulla-Menashe, D., Woodcock, C.E., Sonnentag, O., Keeling, R.F., Friedl, M. A., 2020. Extensive land cover change across Arctic–Boreal Northwestern North America from disturbance and climate forcing. Global Change Biol. 26 (2), 807–822. https://doi.org/10.1111/gcb.14804.
Wear, D.N., Greis, J.G., 2002. Southern forest resource assessment: Summary of findings. J. Forestry 100 (7), 6–14.
Williams, A.P., Allen, C.D., Millar, C.I., Swetnam, T.W., Michaelsen, J., Still, C.J., Leavitt, S.W., 2010. Forest responses to increasing aridity and warmth in the southwestern United States. Proc. Natl. Acad. Sci. 107 (50), 21289–21294.
Williams, Park, A., Cook, I., B., Smerdon, J.E., Bishop, D.A., Seager, R., Mankin, J.S, 2017. The 2016 southeastern US drought: An extreme departure from centennial wetting and cooling. J. Geophys. Res.: Atmospheres 122 (20), 10,888-10,905.
Wolf, J., West, T.O., Le Page, Y., Kyle, G.P., Zhang, X., Collatz, G.J., Imhoff, M.L., 2015. Biogenic carbon fluxes from global agricultural production and consumption. Glob. Biogeochem. Cycles 29 (10), 1617–1639.
Woodbury, P.B., Smith, J.E., Heath, L.S., 2007. Carbon sequestration in the US forest sector from 1990 to 2010. Forest Ecol. Manag. 241 (1–3), 14–27.
Wright, C.K., Wimberly, M.C., 2013. Recent land use change in the Western Corn Belt threatens grasslands and wetlands. Proc. Natl. Acad. Sci. 110 (10), 4134–4139. https://doi.org/10.1073/pnas.1215404110.
Yang, L., Jin, S., Danielson, P., Homer, C., Gass, L., Bender, S.M., Case, A., Costello, C., Dewitz, J., Fry, J., 2018. A new generation of the United States National Land Cover Database: Requirements, research priorities, design, and implementation strategies. ISPRS J. Photogramm. Remote Sens. 146, 108–123.
Yu, Z., Lu, C., 2018. Historical cropland expansion and abandonment in the continental U.S. during 1850 to 2016. Global Ecol. Biogeogr. 27 (3), 322–333. https://doi.org/10.1111/geb.12697.
Yu, Z., Lu, C., Tian, H., Canadell, J.G., 2019. Largely underestimated carbon emission from land use and land cover change in the conterminous United States. Global Change Biol. 25 (11), 3741–3752. https://doi.org/10.1111/gcb.14768.
Zhang, Y., Song, C., Zhang, K., Cheng, X., Band, L.E., Zhang, Q., 2014. Effects of land use/land cover and climate changes on terrestrial net primary productivity in the Yangtze River Basin, China, from 2001 to 2010. J. Geophys. Res.: Biogeosci. 119 (6), 1092–1109.
Zhang, Y., Song, C., Sun, G., Band, L.E., McNulty, S., Noormets, A., Zhang, Q., Zhang, Z., 2016. Development of a coupled carbon and water model for estimating global gross primary productivity and evapotranspiration based on eddy flux and remote sensing data. Agric. For. Meteorol. 223, 116–131.
Zhang, Y., Song, C., Band, L.E., Sun, G., Li, J., 2017. Reanalysis of global terrestrial vegetation trends from MODIS products: Browning or greening? Remote Sens. Environ. 191, 145–155.
Zhang, Y., Song, C., Band, L.E., Sun, G., 2019. No proportional increase of terrestrial gross carbon sequestration from the greening Earth. J. Geophys. Res.: Biogeosci. 124 (8), 2540–2553.